PHYSICAL REVIEW B
CONDENSED MATTER

THIRD SERIES, VOLUME 43, NUMBER 2 15 JANUARY 1991-I

Unoccupied energy bands, exchange splitting, and self-energy of iron

A. Santoni* and F. J. Himpsel
IBM Research Division, Thomas J. Watson Research Center, P.O. Box 218, Yorktown Heights, New York 10598
(Received 25 June 1990; revised manuscript received 15 November 1990)

Unoccupied energy bands of iron are mapped by inverse photoemission from Fe(100), Fe(110), and Fe(111). The ferromagnetic exchange splitting δE_{ex} of the uppermost d band is measured for the H'_{25} point, where the minority- and majority-spin subbands are both empty ($\delta E_{ex}=1.8$ eV with $H'_{25\downarrow}$ at 1.9 eV and $H'_{25\uparrow}$ at 0.12 eV above E_F). Several other critical points are determined, such as the minority-spin Γ_{12} and P_3 points, the majority-spin N_3 point, and the higher-lying H_{15},H_1 points of s,p character. Critical points and exchange splitting are compared with first-principles, local-density calculations. The real part of the self-energy is obtained from this comparison, and the imaginary part by measuring the lifetime broadening. In the d-band region, the self-energy causes a 10% compression of the bands and a linear broadening $\Gamma(E)\approx 0.6|E-E_F|$.

INTRODUCTION

Iron is the classic ferromagnet and one of the most common materials. It has served as a model for itinerant, i.e., bandlike ferromagnetism. The occupied bands of Fe have been studied extensively with angle-resolved photoemission, but only little information is available about the unoccupied bands. Photoemission data[1–11] on the band dispersions and the ferromagnetic exchange splitting δE_{ex} of Fe are close to first-principles band calculations using the local-density method. For Ni, by contrast, the observed bandwidth is narrower than calculated and the exchange splitting is much smaller.[4,12,13] Cobalt lies in between.[14] The unoccupied bands of ferromagnets are of particular interest, since they contain the unbalanced minority-spin holes that make up the magnetic moment. They are accessible through inverse photoemission (for reviews, see Refs. 15–17). However, there has been relatively little work on the unoccupied energy bands of ferromagnets. They have been seen in Ni, Co, and Fe, but the information about band dispersions along symmetry lines is very scarce and no critical points have been reported (for Ni and Co, see reviews;[15–17] for Fe see Refs. 18 and 19). Insufficient tunability of the photon energy has made it difficult to reach high-symmetry points in **k** space. We have used a tunable inverse photoemission spectrograph to map energy bands of Fe. The ferromagnetic exchange splitting is resolved exceptionally well near the H'_{25} point, better than in any photoemission or inverse photoemission work on Fe, Co, and Ni to date. The observed band dispersions and critical points are compared with first-principles, local-density band calculations in order to show self-energy effects.

EXPERIMENT

Fe(100), Fe(110), and Fe(111) crystals were cleaned by established procedures.[20,21] An initial heat treatment in 1 atm of H_2 for about a day (with the temperature varied between 400 and 700 °C) was followed by sputter-annealing cycles. The last anneal was kept short (flashing to 700 °C with about 1 min cooling time) in order to prevent outdiffusion of residual impurities. Sharp 1×1 low-energy electron diffraction (LEED) patterns were seen at this point. The inverse photoemission spectra were taken after transferring the sample in vacuum from the preparation chamber to the spectrometer chamber, with a pressure in the mid-10^{-11} Torr range.

We used a high-resolution inverse photoemission spectrograph[22] with an energy resolution of 0.27 eV at low energies. An accurate line shape was obtained by taking the derivative of the Fermi edge for a material with roughly constant density of states near the Fermi level, such as oxidized tantalum (cf. Ref. 23). The spectrograph detects a range of emitted photon energies, while the initial energy of the electron E_i is fixed. Thereby, the initial

momentum of the electrons is the same over the whole spectrum.

SELECTION RULES AND FREE-ELECTRON BANDS

All data were taken with the electron beam incident normal to the surface ($\mathbf{k}^{\parallel}=0$), and with the photons taken off unpolarized at 45° from the sample normal. Consequently, the electric field component **E** parallel to the surface has a three times higher detection probability than the perpendicular component. At $\mathbf{k}^{\parallel}=0$, one sees the $\Gamma\Delta H$ line on the (100) surface, the $\Gamma\Sigma N$ line on the (110) surface, and the $\Gamma\Lambda PFH$ line on the (111) surface (see Fig. 1 and Ref. 24). The incident electron is in a Δ_1,Σ_1, and Λ_1,F_1 state, respectively, since these are the only states without a node along the surface normal. Dipole selection rules[25,26] dictate the possible final states, which are Δ_5 [**E** parallel to the (100) surface], Δ_1 [**E** perpendicular to the (100) surface], Σ_3,Σ_4 [**E** parallel to the (110) surface], Σ_1 [**E** perpendicular to the (110) surface], $\Lambda_3\mathbf{F}_3$ [**E** parallel to the (111) surface], and Λ_1,F_1 [**E** perpendicular to the (111) surface].

While the wave vector component parallel to the surface $\mathbf{k}^{\parallel}$ is fixed at zero in our experiment, the perpendicular component $k^{\perp}$ is varied by changing the initial energy E_i of the incoming electrons and, consequently, the photon energy of the transitions. E_i can be converted into $k^{\perp}$ using the band dispersion $E_i(k^{\perp})$ of the initial state band, as discussed in more detail in the band structure section. The main features of the initial state band can be understood in terms of the "primary cone", i.e., a free-electron-like band, backfolded by reciprocal lattice vectors perpendicular to the surface. In our energy range, its key features are the following (see Figs. 1 and 5): For the (100) surface, the primary cone corresponds to the Δ_1 bands. The free electron parabola encounters the zone boundary at H, where a large gap opens up (almost 10 eV). We use the edges of this gap to probe the H points. Inside the gap, the real part of $k^{\perp}$ is close to the H point, but a substantial imaginary part smears $k^{\perp}$ along the ΓH line. The (110) surface has the shortest distance to the zone boundary (ΓN), reflecting its close-packed structure. The corresponding zone boundary gap of the free-electron band at N straddles the vacuum level, allowing us to probe the N point at its upper end. The back-folded branch returns to Γ at about 30 eV above E_F, providing the lowest possible initial state at Γ for any surface. For that reason, Fe(110) was chosen to determine Γ in our work. On the (111) surface, the primary cone crosses P near 10 eV, coming from Γ and moving on to H. Note that the primary cone is not reflected back at P since $2\Gamma P=(2\pi/a)[111]$ is not a reciprocal lattice vector. The smallest reciprocal lattice vector in the [111] direction is twice as large and corresponds to $2\Gamma PH=(2\pi/a)[222]$ (see Fig. 1 and Refs. 24 and 27). Thus, one has to go through more than one Brillouin zone before the primary cone is backreflected. This is a characteristic of the open surfaces, i.e., (111) in the body-centered-cubic bcc lattice and (110) in the face-centered-cubic fcc lattice.

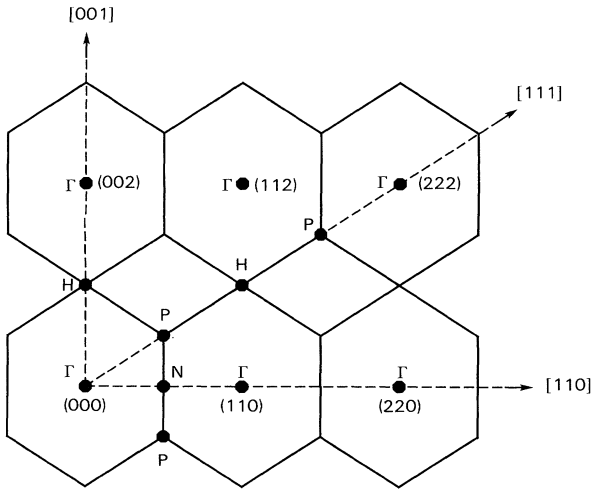

FIG. 1. Cut through a repeated zone scheme of the bcc reciprocal lattice, showing the regions of **k** space seen for various surfaces (after Ref. 24). Note that along the [111] direction, there are contributions from two Brillouin zones along the $\Gamma\Lambda P$ and PFH lines, respectively. The spectra discussed here cover the region from the boundary of the first Brillouin zone (at low initial energies) until halfway into the second Brillouin zone (at high energies). The unit for **k** is $2\pi/a$.

INVERSE PHOTOEMISSION RESULTS

Inverse photoemission spectra from Fe(100), Fe(110), and Fe(111) are shown in Figs. 2–4. They represent the critical points that we have mapped. These and the available photoemission results on critical points and their ex-

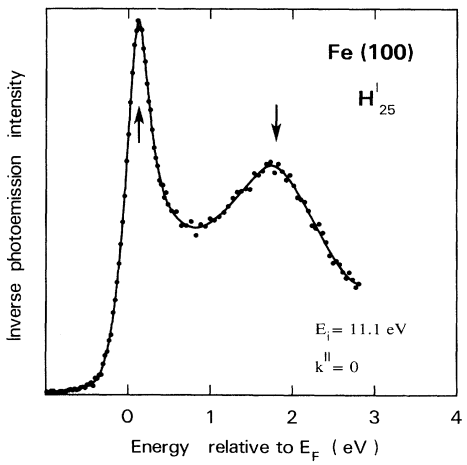

FIG. 2. Inverse photoemission spectrum from Fe(100) showing the majority and minority spin bands at the H'_{25} point, respectively. The ferromagnetic exchange splitting is $\delta E_{ex}=1.8$ eV.

change splittings are compiled in Table I. A particularly clear-cut situation is encountered for Fe(110) at an initial energy of $E_i = 11.1$ eV above the Fermi level E_F (Fig. 2). At this energy, the transitions take place close to the high-symmetry point H, from an initial state near H_{15} to final states at the majority and minority spin H'_{25} points (cf. Fig. 5 and the discussion below). Since there are no other possible final states, the ferromagnetic exchange splitting δE_{ex} is resolved very well. The data were fitted by Lorentzians, broadened by the experimental resolution function, which has been determined by taking the derivative of the Fermi edge of Ta (see Ref. 23). The main uncertainty in this fit turned out to be the choice of the secondary photon background. A splitting $\delta E_{ex} = 1.8$ eV is obtained with energies $E_\downarrow = 1.9$ eV and $E_\uparrow = 0.12$ eV and Lorentzian widths $\Gamma_\downarrow = 0.9$ eV and $\Gamma_\uparrow = 0.09$ eV (full width at half-maximum). These widths reflect the lifetime broadening (or imaginary part of the self-energy) of the final state. Additional broadening mechanisms add

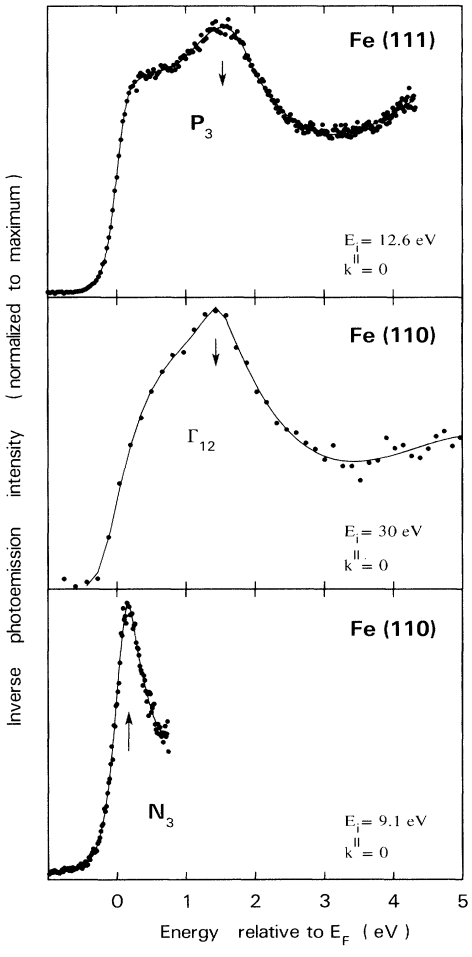

FIG. 3. Inverse photoemission spectra from Fe(111) and Fe(110) showing the minority spin band at P_3 and Γ_{12} and the majority spin band at N_3.

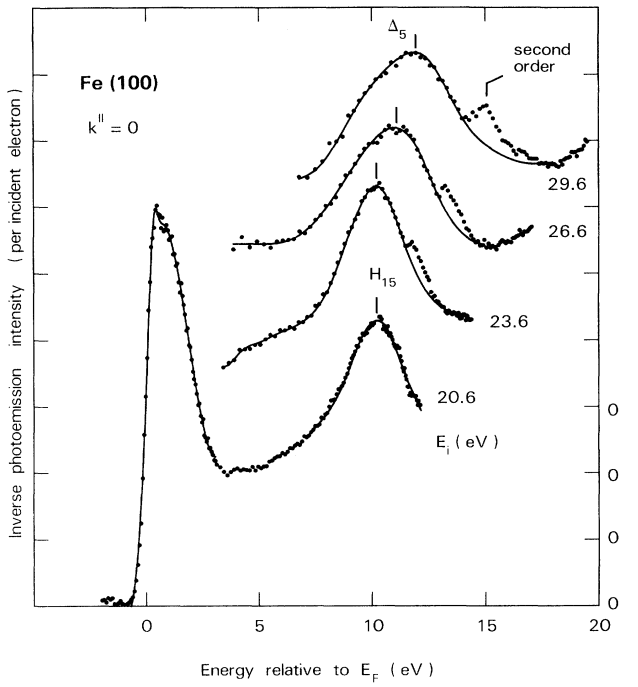

FIG. 4. Inverse photoemission spectra from Fe(100) showing the dispersion of a higher-lying Δ_5 band of s,p character with its minimum at H_{15}.

to the width at higher initial state energies, e.g., the $k^\perp$ broadening of the evanescent initial state in the $H_{15}-H_{12}$ band gap and the deteriorating energy and momentum resolution of the spectrometer. At initial energies above 21 eV, one leaves the band gap and moves back to Γ along the Δ line (see Fig. 1 and marks on top of Fig. 5). A higher-lying Δ_5 band of s,p character can be picked up, which disperses upwards from the H_{15} point (Figs. 4 and 5). Its minimum at 10.2 eV defines the H_{15} point. Here it is seen as the final state, while it was the initial state for the spectrum in Fig. 2. The initial energy of the H_{15} transition in Fig. 4 (about 21 eV) marks H_1 and the nearby H_{12} point. Lifetime broadening at these energies is too large to separate them. The position of H_{12}, H_1 is located by observing the dispersion of the Δ_5 band going to zero at an initial energy of about 21 eV. Additional clues for the edges of the $H_{15}-H_{12}$ band gap come from the drop in intensity that interband transitions undergo when the initial state moves into the gap. The Δ_5 H_{15} transition in Fig. 4 loses strength for E_i smaller than 21 eV because the upper state moves into the gap. Likewise, the H'_{25} transition in Fig. 2 decreases in intensity for E_i higher than 11 eV because the upper state lies in the gap. By contrast, the transitions on the Fe(111) surface become stronger with increasing E_i due to the increasing cross section of $3d$ states.

For Fe(110), the band structure is rather complex due to the low symmetry along the Σ line (see Ref. 28). Here we concentrate on the critical points, where the situation is relatively clearcut (Fig. 3). The Γ_{12} point can be seen at initial energies 30 eV, which are just barely reachable with a normal incidence spectrograph. For improving the resolution, we have taken the data in second diffraction order. At the other end of the spectrum is the N point, which is reached at an initial energy of about 8 eV (see Table I). It exhibits two groups of empty bands (see Table I). The upper group consists of the N_3, N_4, and N_1 minority spin bands, which are seen as an unresolved structure between 1.5 and 2.0 eV above E_F (not shown). The lower group contains the N_3 majority spin band and the s,p-like N_1' minority and majority spin bands. They appear at initial energies below 11 eV, where they cross the Fermi level (compare the band structure in Ref. 28 and Fermi surface data in Ref. 29). Going towards the lower limit of our spectral range (Fig. 3), we see a peak dispersing upwards through the Fermi level. The assignment of this feature to either the $N_3\uparrow$ or $N_1'\uparrow\downarrow$ points is not easy. On one hand, the transition be-

TABLE I. Critical points and ferromagnetic exchange splitting δE_{ex} of Fe (energies in eV with respect to the Fermi level). $\uparrow$ = majority spin, $\downarrow$ = minority spin, $\uparrow\downarrow$ = average.

Critical point	E experiment	E calculation[a]	δE_{ex} experiment	δE_{ex} calculation[a]
$\Gamma_1\uparrow\downarrow$	−8.15[b]	−8.12		0.17
$\Gamma_{25}'\uparrow$	−2.35,[b] −2.6,[c] −2.55[e]	−2.25	2.14[g]	1.82
$\Gamma_{25}'\downarrow$	−0.27,[b] −0.4,[c] −0.41[e]	−0.43	2.14[g]	1.82
$\Gamma_{12}\uparrow$	−0.78,[b] −1.2,[c] −0.61[e]	−0.86	2.4[f,g]	2.18
$\Gamma_{12}\downarrow$	+1.5[f]	+1.32	2.4[f,g]	2.18
$\Gamma_{15}\uparrow\downarrow$		+32.4		0.75
$\Gamma_{25}'\uparrow\downarrow$		+32.7		0.87
$H_{12}\uparrow$	−3.8[b]	−4.50	1.3[b]	1.51
$H_{12}\downarrow$	−2.5[b]	−2.99	1.3[b]	1.51
$H_{25}'\uparrow$	+0.12[f]	+0.11	1.8[f]	2.11
$H_{25}'\downarrow$	+1.9[f]	+2.22	1.8[f]	2.11
$H_{15}\uparrow\downarrow$	+10.2[f]	+9.70		0.28
$H_{12}\uparrow\downarrow$	+21[f]	+18.9		1.16
$H_1\uparrow\downarrow$	+21[f]	+21.2		0.79
$P_4\uparrow$	−3.20,[b] −3.0[d]	−3.17	1.35,[b] 1.5[d]	1.34
$P_4\downarrow$	−1.85,[b] −1.5[d]	−1.83	1.35,[b] 1.5[d]	1.34
$P_3\uparrow$	−0.60,[b] −0.5[d]	−0.53	2.1[d,f]	2.10
$P_3\downarrow$	+1.6[f]	+1.57	2.1[d,f]	2.10
$P_4\uparrow\downarrow$		+8.82		0.92
$P_1\uparrow\downarrow$		+11.0		0.56
$N_1\uparrow$	−4.50,[b] −4.16[e] $\uparrow\downarrow$	−4.75	0.90[b]	1.65
$N_1\downarrow$	−3.60,[b] −4.16[e] $\uparrow\downarrow$	−3.60	0.90[b]	1.65
$N_2\uparrow$	−3.00[b]	−3.27	1.60[b]	1.65
$N_2\downarrow$	−1.40[b]	−1.62	1.60[b]	1.65
$N_1\uparrow$	−0.70,[b] −1.02[e]	−0.86		2.11
$N_1\downarrow$		+1.25		2.11
$N_4\uparrow$	−0.70[b]	−0.69		2.23
$N_4\downarrow$		+1.54		2.23
$N_1'\uparrow$		+0.40		0.16
$N_1'\downarrow$		+0.56		0.16
$N_3\uparrow$	+0.4[f]	+0.38		2.14
$N_3\downarrow$		+2.52		2.14
$N_1\uparrow\downarrow$		+7.88		1.26

[a]Local-density calculation with the von Barth Hedin potential from Callaway and Wang (Ref. 28).
[b]Photoemission (Ref. 8) (see also Ref. 6).
[c]Photoemission (Ref. 10) (see also Ref. 9).
[d]Photoemission (Ref. 4).
[e]Photoemission (Ref. 11).
[f]Inverse photoemission (this work).
[g]The average among b, c, and e.

tween the N_1 upper state and N_3 is dipole forbidden, while the transition between N_1 and N_1' is allowed.[26] On the other hand, the N_1' s,p band disperses very rapidly and should give a much broader peak than the flat N_3 d band, given finite momentum broadening. We tend towards the assignment as the N_3 point, using previous experience with a similar situation for Ni(111) and Co(0001), which are close-packed analogs to the (110) face of the bcc lattice. The corresponding critical points are the s,p-like L_2' point and the d-like L_3 point, with a L_1 upper state (see Refs. 13 and 14). The selection rules at L and N are similar (transitions are only allowed between primed and nonprimed states[26]). Nevertheless, the L_3 d band dominates over the L_2' s,p band.[13,14] The breaking of the selection rules can be explained by spin–orbit interaction, or by the sampling of k points away from the high-symmetry point L. For the case of Fe(110), our limited photon energy range allows us only to go 2 eV above the $N_1\uparrow$ initial state along the Σ axis, where the transition is still allowed. In order to obtain the correct energy of the N point, the measured final state energy of 0.16 eV has to be extrapolated. By using calculated bands[28] for the $\Sigma_1\uparrow$ initial state and taking into account the calculated dispersion of the final state, one obtains a final energy of 0.4 eV for the extrapolated $N_3\uparrow$ point.

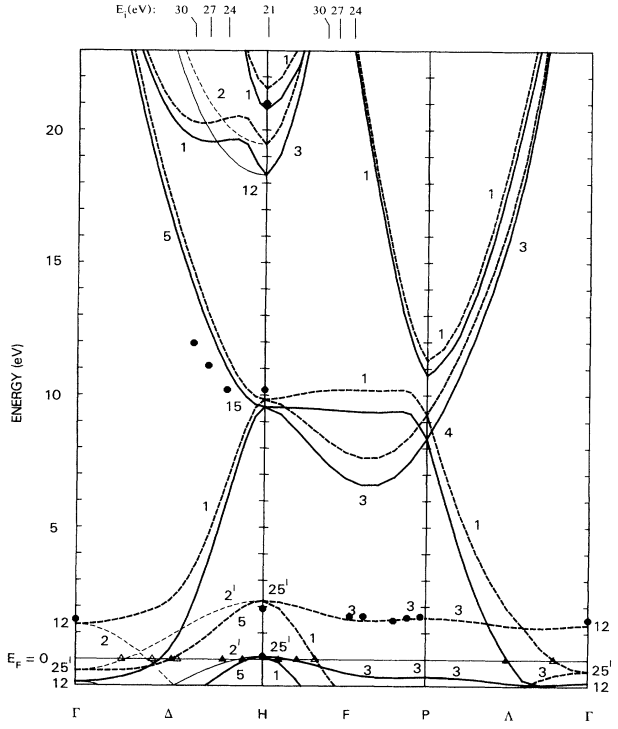

FIG. 5. Energy band dispersions of Fe along the [100] and [111] high symmetry lines. Full dots are from this work, triangles from Fermi surface data (Ref. 29, open for minority, full for majority spin), and lines from a local density calculation (Ref. 28). Full (dashed) lines stand for majority (minority) spin and fat (thin) lines for allowed (forbidden) transitions at $\mathbf{k}^{\parallel}=0$. The energy marks on top of the figure give the continuation of the free-electron-like initial state for higher energies.

At the Fe(111) surface (Fig. 3) a single feature is observed 1.6 eV above E_F with a full width at half-maximum of $\Gamma_{\downarrow}=0.9$ eV. It corresponds to the minority spin band near the P_3 point (cf. Fig. 5). The corresponding majority spin band is occupied and has been observed in photoemission[4] at -0.5 eV. The resulting exchange splitting is $\delta E_{ex}=2.1$ eV.

An additional feature on Fe(110) and Fe(111) is a sharp peak at 4.5 and 4.05 eV, respectively (not shown). Fe(100) exhibits only a weak trace of it. This feature is assigned to an image potential surface state (see Ref. 43 for details and Refs. 15–17 for reviews). The energy fits well to a reported work function of 4.81 eV (Ref. 30) for Fe(111), resulting in a binding energy of 0.76 eV. Such a value is typical for inverse photoemission from image states on metal surfaces.[31] The state disperses rapidly upwards away from the zone center. The intensity of the image state is strongest for Fe(110), since it falls into a band gap for this surface. Image-state spectra and a discussion of the magnetic splitting of image states will be reported elsewhere.[43]

BAND STRUCTURE AND EXCHANGE SPLITTING

Band dispersions are obtained (Fig. 5) by using the dispersion of the initial state band $E_i(k^{\perp})$ to obtain $k^{\perp}$ for the final state. We use semiempirical initial state bands, which consist of calculated bands with their critical points adjusted to the extrema in the observed band dispersions. This method has been successful[13,14,16] in mapping the energy bands of Ni and many other materials. For initial state energies below 20 eV, the Δ_1, Σ_1, Λ_1, F_1 bands of the local density calculation by Callaway and Wang[28] are taken. They happen to reproduce the experimental H_{15},H_1 points reasonably well (Fig. 5). For high energies, we also take a LEED-type calculation by Jepsen[32] into account, which includes smearing out of miniband gaps by the finite lifetime broadening. Initial state bands beyond the energy range of Fig. 5 are indicated by marks on top of the figure. The experimental energy bands are given by dots in Fig. 5.

From the data, one can derive the ferromagnetic exchange splitting at several points in the Brillouin zone (see Table I). The inverse photoemission results make it possible to obtain the exchange splitting not only between occupied bands, as previously available, but also between occupied–empty and empty–empty bands. Thus the influence of the charge state on the exchange splitting can be seen, which would make a big difference in localized systems. For an itinerant ferromagnet such as Fe, there is very little effect of the charge state on the exchange splitting, in agreement with a previous finding for Co (see Ref. 16). The variations between different critical points are more likely to be attributed to a momentum and symmetry dependence of the exchange splitting.

SELF-ENERGY

For understanding the band-structure concept, it is important to realize that traditional band-structure calculations produce energy eigenvalues that apply to the ground state only. In principle, they have no relationship to the measured bands, which necessarily involve the creation of an excited state (e.g., a hole in photoemission and an electron in inverse photoemission). The difference between the quasiparticle energies in the excited state and the calculated ground state energies can be summarized by the self-energy. The real part of the self-energy gives the energy shifts, while the imaginary part describes the width of the states induced by the finite lifetime of the excited state. In recent years, it has become possible to calculate the self-energy by solving the Dyson equations for the electron and photon propagators which describe the fully interacting many-electron system.[33] Although such quasiparticle band calculations have not yet been performed for Fe, there exists a cluster approach[34] of the problem. Other excited state calculations have been performed for nearby elements, such as Ni (Ref. 35) and Cr (Ref. 36).

The self-energy obtained from our inverse photoemission experiment and from previous photoemission data is summarized in Fig. 6 for the region of the 3*d* bands. The real part of the self-energy can be approximated roughly by a straight line through the origin with a slope of -0.1,

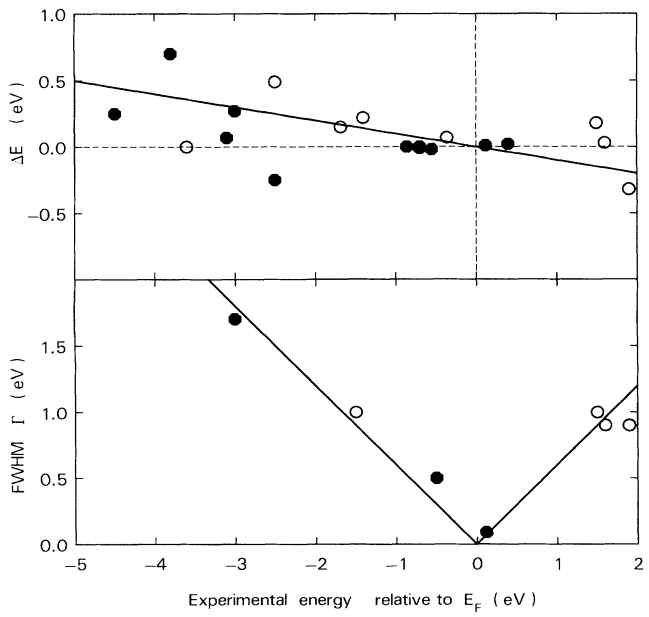

FIG. 6. Energy differences ΔE and widths Γ for *d*-band critical points of Fe, representing the real and imaginary parts of the self-energy, respectively. ΔE equals the experimental energy minus the local density eigenvalue (from Table I, Refs. 4, 6, 8–10, 28, and this work, after taking an average of multiple experimental results). Γ equals the full width at half-maximum from Ref. 4 and this work. Full (open) symbols are for the majority (minority) spin, respectively. The data are summarized by drawing straight lines through the origin with a slope of -0.1 for $\Delta E(E)$ and ± 0.6 for $\Gamma(E)$.

corresponding to a 10% narrowing of the *d* bands. Qualitatively, this is the same effect as observed in other transition metals (for a review, see Ref. 37). Here we have the new capability of testing the self-energy above the Fermi level. There is large scatter in the data between different critical points. That is partly experimental, as the variations in the photoemission energies from different groups attest (see Table I). There are also some more general obstacles. Momentum broadening by the finite lifetime of the upper band shifts the energies of rapidly dispersing bands (we chose critical points to minimize this effect). It should be noted that the self-energy does not have to be a smooth function of the energy of critical points. It also depends on the character of the wave function. Anomalies in the self-energy have been seen in semiconductors[23] for states with unusual spatial charge distribution.

For the imaginary part of the self-energy, i.e., the lifetime broadening (bottom of Fig. 6), there exist very few data points. At any rate, they may be crudely summarized by a linear function of the energy distance from the Fermi level with a slope of 0.6, i.e., the broadening is 0.6 times the energy from the Fermi level. Traditionally, the lifetime broadening has always been assumed to increase quadratically away from the Fermi level, based on the phase space available for electron–hole-pair creation in an electron gas and on resistivity data. However, a linear behavior has been calculated in some instances (cf. Refs. 35 and 36). It has been observed for the 3*d* bands of Ni (Ref. 38) and of Cu in high temperature superconductors (Ref. 39). In the latter case, a slope of 0.6 was found, identical to our value for iron. This linear behavior has stimulated much theoretical interest, with models ranging from a modest "marginal Fermi liquid" to more exotic phases of matter. Since we are dealing with 3*d* electrons in iron as well as in high temperature superconductors, there may be a real connection between the lifetime data. A less exotic explanation of the linear lifetime curve comes from a more detailed study of the density of states. The quadratic dependence holds only for a constant density of states around the singularities near the Fermi level. If there is a δ function of states at the Fermi level, the lifetime becomes linear[38,40] Since the density of the 3*d* bands contains sharp peaks, a linear behavior may not be that unexpected, at least not for energies far enough away from the singularities near the Fermi level.

The higher-lying *s*,*p* bands behave differently from the 3*d* bands, i.e., they are expanded relative to the local density band calculation. In a highly simplified picture, one can argue that the attractive crystal potential is reduced at high kinetic energies. The faster the excited electron, the less it feels the response of the crystal electrons. This effect can be simulated by a constant self-energy stretch of the higher-lying bands, at least for the energy region probed in our experiment. In Cu a stretch of 7% has been obtained.[41,42] If we take the H_{15} point for Fe (cf. Table I), we obtain a 5% stretch.

SUMMARY

In summary, the critical points of unoccupied energy bands of iron have been measured. They are used togeth-

er with the available photoemission data to characterize the band dispersion and the ferromagnetic exchange splitting, thereby giving a complete picture of the electronic structure. Particularly striking is the well-resolved ferromagnetic exchange splitting at the H'_{25} point. In order to study higher order excited state effects on the band structure, we have also determined the lifetime broadening (corresponding to the imaginary part of the self-energy) and the disrepancy between experimental and calculated ground state band energies (corresponding to the real part of the self-energy). It is interesting to note that the lifetime broadening is linear in energy with a slope of 0.6, i.e., equal to that observed for the states near the Fermi level in high temperature superconductors. The real part of the self-energy corresponds to an average d-band narrowing of 10%. Surface effects show up mainly via the appearance of image states. It would be interesting to further pursue the magnetic properties of the observed image states,[43] particularly a possible magnetic splitting. This would be a first step for creating a spin-polarized, two-dimensional electron gas.

ACKNOWLEDGMENTS

We would like to acknowledge F. Jona for lending us a Fe(100) crystal, J. Callaway and D. W. Jepsen for providing unpublished band-structure results, and J. Yurkas for help with the experimental setup. One of the authors (A.S.) would like to gratefully acknowledge the Max Planck Gesellschft for support.

*Permanent address: ENEA, TIB, c/o Sincrotrone Trieste, Padriciano 99, 30412 Trieste, Italy.

[1]P. Heimann and H. Neddermeyer, Phys. Rev. B **18**, 3537 (1978).

[2]S. D. Kevan, P. S. Wehner, and D. A. Shirley, Solid State Commun. **28**, 517 (1978).

[3]A. Schulz, R. Courths, H. Schulz, and S. Hüfner, J. Phys. F **9**, L41 (1979).

[4]D. E. Eastman, F. J. Himpsel, and J. A. Knapp, Phys. Rev. Lett. **44**, 95 (1980).

[5]A. M. Turner, Yu. Jeng Chang, and J. L. Erskine, Phys. Rev. Lett. **48**, 348 (1982).

[6]A. M. Turner and J. L. Erskine, Phys. Rev. B **25**, 1983 (1982).

[7]R. Feder, W. Gudat, E. Kisker, A. Rogriguez, and K. Schröder, Solid State Commun. **46**, 619 (1983).

[8]A. M. Turner, A. D. Donoho, and J. L. Erskine, Phys. Rev. B **29**, 2986 (1984).

[9]E. Kisker, A. Schröder, M. Campagna, and W. Gudat, Phys. Rev. Lett. **52**, 2285 (1984).

[10]E. Kisker, K. Schröder, W. Gudat, and M. Campagna, Phys. Rev. B **31**, 329 (1985).

[11]Y. Sakisaka, Thor. Rhodin, and D. Mueller, Solid State Commun. **53**, 793 (1985).

[12]D. E. Eastman, F. J. Himpsel, and J. A. Knapp, Phys. Rev. Lett. **40**, 1514 (1978).

[13]F. J. Himpsel, J. A. Knapp, and D. E. Eastman, Phys. Rev. B **19**, 2919 (1979).

[14]F. J. Himpsel and D. E. Eastman, Phys. Rev. B **21**, 3207 (1980).

[15]V. Dose, Surf. Sci. Rep. **5**, 337 (1985).

[16]F. J. Himpsel, Comments Condensed Matter Phys. **12**, 199 (1986).

[17]N. V. Smith, Rep. Prog. Phys. **51**, 1227 (1988).

[18]H. Scheidt, M. Glöbl, and V. Dose, Phys. Rev. Lett. **51**, 1688 (1983).

[19]J. Kirschner, M. Glöbl, V. Dose, and H. Scheidt, Phys. Rev. Lett. **53**, 612 (1984).

[20]J. Kirschner, Surf. Sci. **138**, 191 (1984).

[21]M. Grunze, G. Strasser, and O. Elshazly, J. Vac. Sci. Technol. A **4**, 2396 (1986).

[22]Th. Fauster, D. Straub, J. J. Donelon, D. Grimm, A. Marx, and F. J. Himpsel, Rev. Sci. Instrum. **56**, 1212 (1985).

[23]F. J. Himpsel, Surf. Sci. Rep. **12**, 1 (1990).

[24]R. F. Willis and B. Feuerbacher, Surf. Sci. **53**, 144 (1975).

[25]H. Hermanson, Solid State Commun. **22**, 9 (1977).

[26]W. Eberhardt and F. J. Himpsel, Phys. Rev. B **21**, 5572 (1980); **23**, 5650 (1981).

[27]There exist additional bands along the ΓP direction, corresponding to "secondary cones" induced by the [211] reciprocal-lattice vectors. However, their slope is smaller than that of the primary cone, which involves the [222] reciprocal-lattice vector. Note that in Figs. 2 and 10 of Ref. 8, the [111] vector has been used to backfold the free-electron band along ΓP, giving an incorrect slope.

[28]J. Callaway and C. S. Wang, Phys. Rev. B **16**, 2095 (1977); J. Callaway (private communication). For similar local-density calculations, see V. L. Moruzzi, J. F. Janak, and A. R. Williams, *Calculated Electronic Properties of Metals* (Pergamon, New York, 1978); D. A. Papaconstantopoulos, *Handbook of the Band Structure of Elemental Solids* (Plenum, New York, 1986); G. A. Prinz, E. Kisker, K. B. Hathaway, K. Schröder, and K.-H. Walker, J. Appl. Phys. **57**, 3024 (1985).

[29]R. V. Coleman, W. H. Lowrey, and J. A. Polo, Jr., Phys. Rev. B **23**, 2491 (1981).

[30]H. Kobayashi and S. Kato, Surf. Sci. **18**, 341 (1969).

[31]D. Straub and F. J. Himpsel, Phys. Rev. B **33**, 2256 (1986).

[32]D. W. Jepsen (unpublished).

[33]L. Hedin and S. Lundqvist, in *Solid State Physics,* edited by F. Seitz, D. Turnbull, and H. Ehrenreich (Academic, New York, 1969), p. 1.

[34]Erik C. Sowa and L. M. Falicov, Phys. Rev. B **35**, 3765 (1987).

[35]D. R. Penn, Phys. Rev. Lett. **42**, 921 (1979); A. Liebsch, *ibid.* **43**, 1431 (1979); L. C. Davis and L. A. Feldkamp, Solid State Commun. **34**, 141 (1980); A. Liebsch, Phys. Rev. B **23**, 5203 (1981); G. Treglia, F. Ducastelle, and D. Spanjaard, *ibid.* **21**, 3729 (1980); J. Phys. (Paris) **43**, 34 (1982); W. Nolting, W. Borgiel, V. Dose, and Th. Fauster, Phys. Rev. B **40**, 5015 (1989).

[36]N. I. Kulikov, M. Alouani, M. A. Khan, and M. V. Magnitskaya, Phys. Rev. B **36**, 929 (1987).

[37]F. J. Himpsel, P. Heimann, and D. E. Eastman, J. Appl. Phys. **52**, 1658 (1981).

[38]W. Eberhardt and E. W. Plummer, Phys. Rev. B **21**, 3245 (1980).

[39]C. G. Olson, R. Liu, D. W. Lynch, R. S. List, A. J. Arko, B. W. Veal, Y. C. Chang, P. Z. Jiang, and A. P. Paulikas, Phys.

Rev. B **42**, 381 (1990).
[40]D. M. Newns, P. C. Pattnaik, and C. C. Tsuei, Phys. Rev. B (to be published).
[41]J. F. Janak, A. R. Williams, and V. L. Moruzzi, Phys. Rev. B **11**, 1522 (1975).
[42]D. E. Eastman, J. A. Knapp, and F. J. Himpsel, Phys. Rev. Lett. **41**, 825 (1978).
[43]F. J. Himpsel (unpublished).